**Supplemental Information Inventory:**

**Supplemental Figures:**

- **Figure S1, Related to Figure 2.** Characterization of germline *Hif1a* KO and validation of anti-HIF1α antibody specificity. Assessment of timing of coronary perfusion by aortic blood flow. Correlation between nuclear HIF1α and fCM proliferation at distinct developmental timepoints.
- **Figure S2, Related to Figure 3.** Evaluation of myocardial recombinase activity at E8.5 and efficiency of HIF1α protein depletion in fCMs using distinct recombinase lines. Cardiac phenotype of surviving *Nkx2-5*$^{WT/Cre}$; *Hif1a*$^{\Delta/fl}$ mutants at E17.5.
- **Figure S3, Related to Figure 4.** In fetal cardiomyocytes HIF1α directly activates expression of MIF, as well as enzymes and transporters involved in each step of glycolysis, but is not required for expression of angiogenic factors.
- **Figure S4, related to Figure 5.** A primary cell culture system that recapitulates *in vivo* consequences of ablation of HIF1α in fetal cardiomyocytes.
- **Figure S5, related to Figure 6.** Diagram listing all genes involved in the cellular processes highlighted in Figure 6.

**Supplemental Tables:**

- **Table S1, related to Figure 1 –** list of Affymetrix microarray datasets used for the elaboration of the heatmap presented in Figure 1.
- **Table S2, related to Figure 4 –** Characterization of the transcriptome of *Hif1a* cKO hearts and assessment of direct gene regulation by HIF1α.
- **Table S3, related to Figure 4 –** Unfiltered list of all 17289 HIF1α ChIP-seq peaks annotated in E12.5 hearts. Data provided in a Excel file.
- **Table S4, related to Figure 4 –** Bioinformatic prediction of putative HIF1α transcriptional partners.
- **Table S5, related to Figure 5 –** Enrichment in ATF4 and p53 target genes amongst genes modulated in *Hif1a* cKO hearts.

**Supplemental Experimental Procedures**

**Supplemental References**

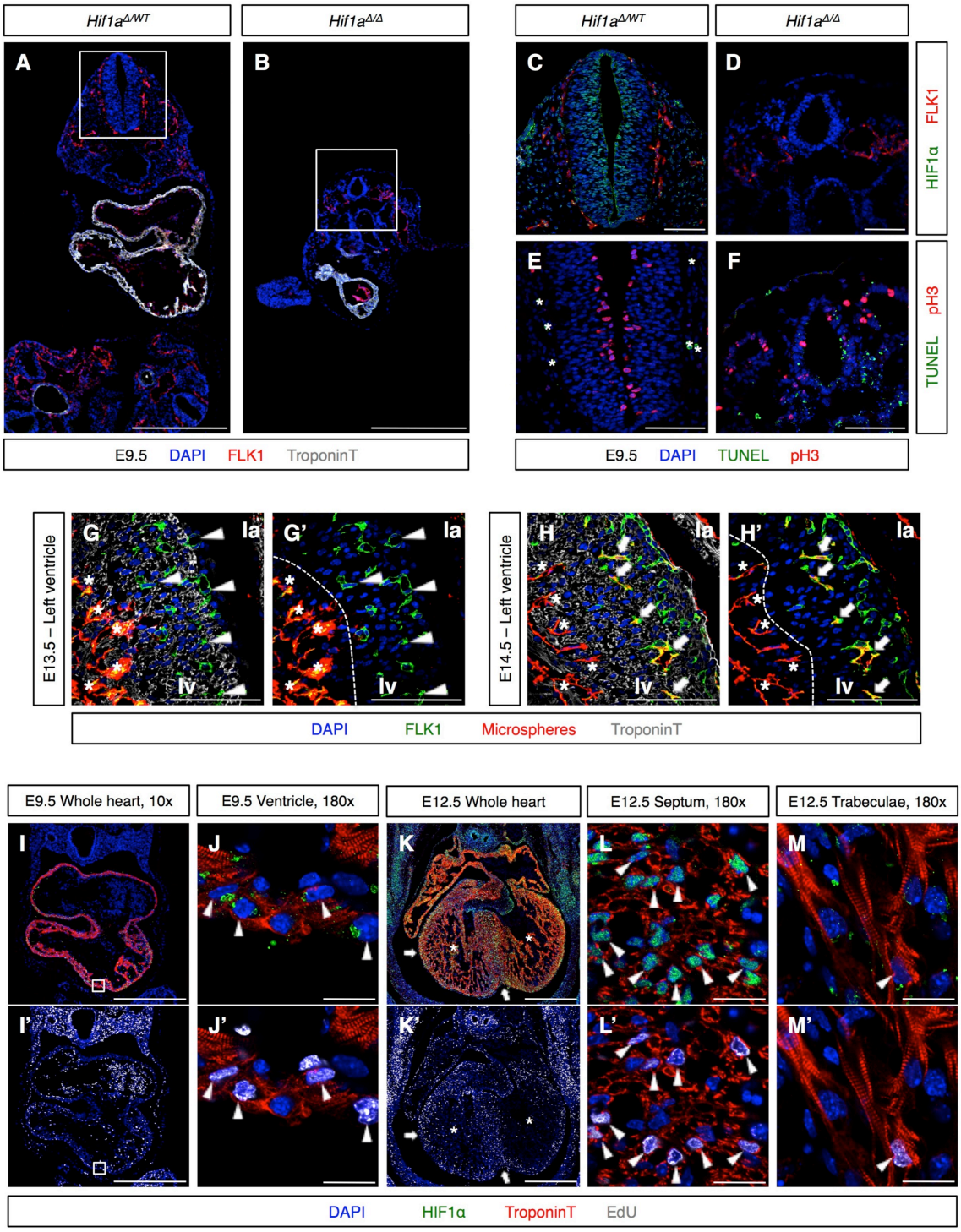


**Figure S1, Related to Figure 2. Characterization of germline *Hif1a* KO and validation of anti-HIF1α antibody specificity. Assessment of timing of coronary perfusion by aortic blood flow. Correlation between nuclear HIF1α and fCM proliferation at distinct developmental timepoints.**

**A to F)** A *Hif1a*$^{\Delta}$ null allele was produced by crossing the floxed *Hif1a* line (Ryan et al., 2000) with an epiblastic Cre, *Meox2*-Cre (Tallquist and Soriano, 2000). *Hif1a*$^{\Delta/WT}$ heterozygotes were interbred and no viable embryos were recovered from E10.5 onwards. **A)** Control (*Hif1a*$^{\Delta/WT}$) and **B)** mutant (*Hif1a*$^{\Delta/\Delta}$) E9.5 embryos. Mutants were much smaller than control littermates, displayed a small, unlooped heart, and severely underdeveloped neural tube. The cardiac hypoplasia is consistent with two previously published *Hif1a* global KOs (Compernolle et al., 2003; Ryan et al., 1998), but distinct from the myocardial hyperplasia reported by Iyer and colleagues (Iyer et al., 1998). **C** and **D** are higher magnification images of areas boxed in A and B, respectively. **C)** The inner cell layers of the wild-type E9.5 neural tube are distal to any vascular structures (marked by FLK1 staining) and exhibited robust nuclear HIF1α staining. **D)** HIF1α staining was undetectable in neural tubes of *Hif1a*$^{\Delta/\Delta}$ embryos, demonstrating the specificity of the anti-HIF1α antibody used in our experiments. **E)** The HIF1α-positive inner cell layer of the neural tube is the area where proliferation of neuronal precursors occurs, as shown by pH3 staining. **F)** This proliferative cell layer was absent in *Hif1a*$^{\Delta/\Delta}$ embryos. Additionally, *Hif1a*$^{\Delta/\Delta}$ embryos displayed an aberrantly high frequency of apoptotic cells in the neural tube and surrounding mesenchymal tissues, as shown by TUNEL staining. *=autofluorescent red blood cells.

**G and H)** To determine the timing at which the developing myocardium gets perfused by oxygenated aortic blood flow, a suspension of 0.1μm orange fluorescent microspheres (red channel) was injected into the left ventricle of embryonic hearts at different stages of development. To allow visualization of endothelial cells, cryosections were immunostained using an anti-FLK1 antibody (green). Yellow/orange color (overlay of FLK1 and microspheres) is observed in endocardium (asterisks) and in coronary vasculature connected to aortic flow. **G)** Dorsal section of an E13.5 heart at the atrio-ventricular sulcus showing that, despite the presence of endothelial cells, the E13.5 left ventricle is not yet perfused by aortic blood flow, as denoted by the absence of FLK1/microsphere co-staining within the left ventricular wall (arrowheads). **H)** 24 hours later, at E14.5, the majority of FLK1-positive cells within the left ventricle co-localized with fluorescent microspheres (arrows) revealing efficient perfusion of the left ventricular wall consequent to the connection of the coronary vascular system to aortic flow. **G'** and **H'** are the same image as **G** and **H**, respectively, where the far-red channel (TroponinT) has been omitted to allow for better visualization of vascular structures. Dashed line

represents the border between trabecular and compact myocardium. la = left atrium, lv = left ventricle.

**I to M)** To understand how nuclear accumulation of HIF1α correlates with fCM proliferation, E9.5 and E12.5 hearts were co-stained for HIF1α and EdU incorporation. Panels I-M display stage and region-specific patterns of HIF1α distribution. Proliferation patterns (EdU incorporation) for the same images are displayed in panels I'-M'. **I,I',J** and **J')** E9.5 fCMs are highly proliferative (arrowheads) but displayed no nuclear accumulation of HIF1α, revealing that at this early developmental timepoint, high rates of fCM proliferation are independent of HIF1α transcriptional control. **J** corresponds to a higher magnification of the area boxed in **I**. **K)** At E12.5 robust nuclear accumulation of HIF1α was detected in the core of the developing ventricular septum and in compact ventricular myocardium (arrows), being largely absent from trabecular myocardium fCMs (asterisks). Interestingly, this distribution positively correlated with fCM proliferative activity (**K'**). **L and L')** High magnification of the core of the ventricular septum demonstrating that fCMs located in this highly proliferative area displayed high levels of nuclear HIF1α. **M and M')** High magnification of left ventricular trabecular myocardium showing that trabecular fCMs preferentially accumulated HIF1α outside their nuclei and displayed reduced, but not absent, proliferative activity. These data show that, although HIF1α nuclear accumulation is not a generic requisite for fCM proliferation, in the specific developmental timepoints during which nuclear HIF1α can be detected in fCMs, presence of this TF directly correlated with high rates of fCM proliferation.

Bars represent 500 μm in A, B, I and K and 50 μm in all other panels.

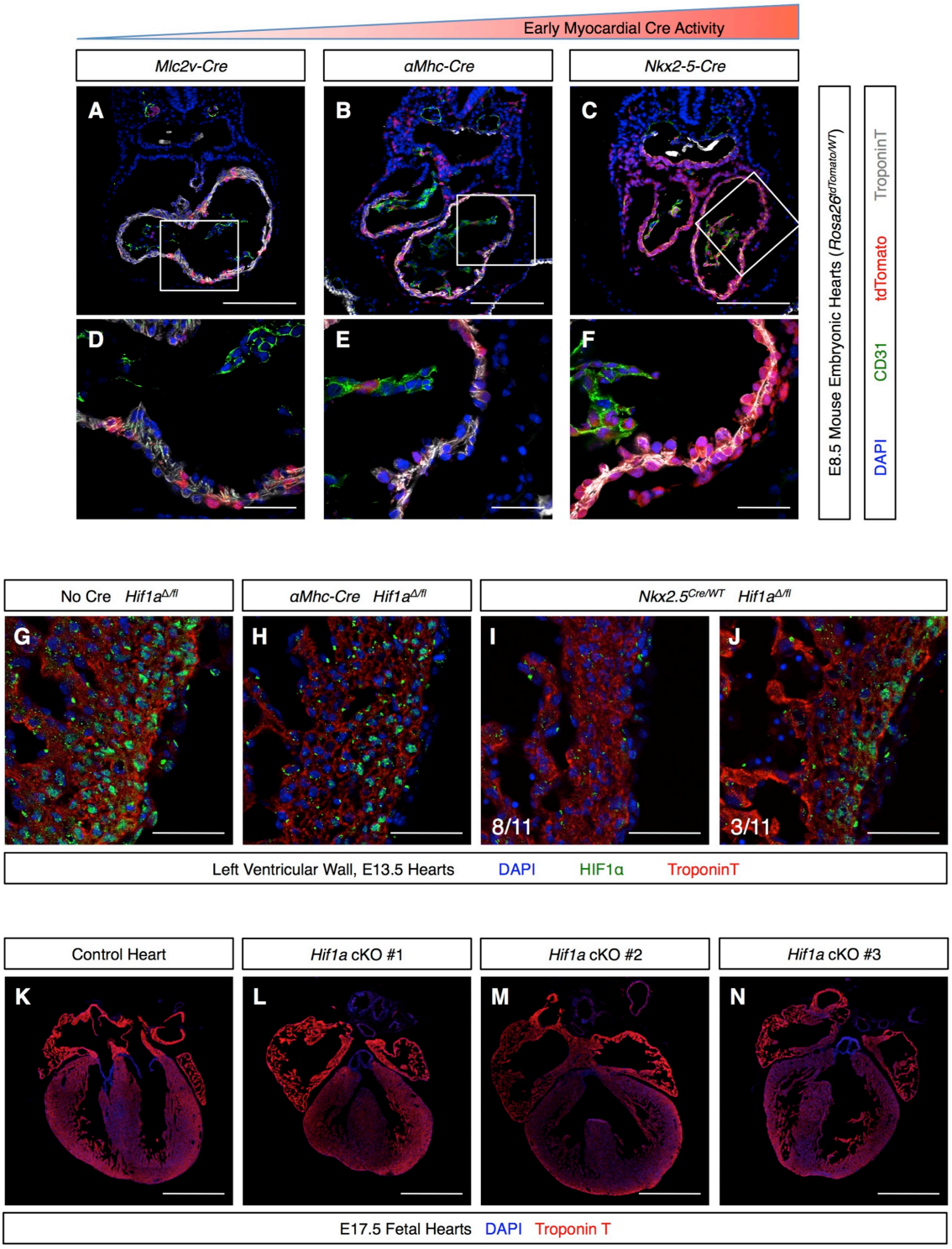


**Figure S2, Related to Figure 3. Evaluation of myocardial recombinase activity at E8.5 and efficiency of HIF1α protein depletion in fCMs using distinct recombinase lines. Cardiac phenotype of surviving *Nkx2-5*$^{WT/Cre}$; *Hif1a*$^{\Delta/fl}$ mutants at E17.5.**

**A to F)** To assess patterns of recombination promoted by different myocardial Cres in early stages of cardiogenesis, animals homozygous for the *Rosa26*$^{tdTomato}$ reporter allele (Madisen et al., 2010) were crossed with three routinely used cardiac Cre lines: *Mlc2v-Cre* (Chen et al., 1998), α*Mhc-Cre* (Abel et al., 1999) and *Nkx2-5-Cre* (Moses et al., 2001). Double transgenic embryos from each cross were isolated at E8.5 and processed for histological analyses using antibodies recognizing the cardiomyocyte (CM) marker TroponinT (gray) and the endothelial cell marker CD31/PECAM (green). **A)** At E8.5 *Mlc2v-Cre* induced recombination of very few ventricular myocytes. No other lineages displayed evidence of recombination. **B)** At a similar stage *αMhc-Cre* labeled approximately half of CMs constituting atrial and ventricular chambers. **C)** *Nkx2-5-Cre* robustly labeled all CMs of both atrial and ventricular chambers. As expected, labeling was not confined to CMs, with endocardial cells, cardiogenic precursors and foregut endoderm also being labeled by this Cre (Moses et al., 2001). **D**, **E** and **F** are higher magnification images of areas boxed in A, B and C, respectively.

**G to J)** The floxed *Hif1a* allele was deleted from mouse embryonic hearts using two distinct myocardial Cre lines: *αMhc-Cre* and *Nkx2-5-Cre.* Consistently with the patterns of early recombinase activity reported in panels A-F, only the latter promoted efficient loss of HIF1α protein. However, even for the *Nkx2-5-Cre* mutants (panels I and J) complete protein ablation was only observed in 73% of mutants, with remaining 27% (3/11) displaying reduced, but not absent HIF1α. Mutants exhibiting inefficient protein depletion were excluded from downstream histological analyses.

**K to N)** Although most *Nkx2-5*$^{WT/Cre}$; *Hif1a*$^{\Delta/fl}$ mutants died before E17.5, a total of three cKOs were recovered at this late gestational stage. When compared with control littermates (**K**), all mutant hearts (**L-N**) exhibited a clear VSD and abnormally shaped ventricular chambers.

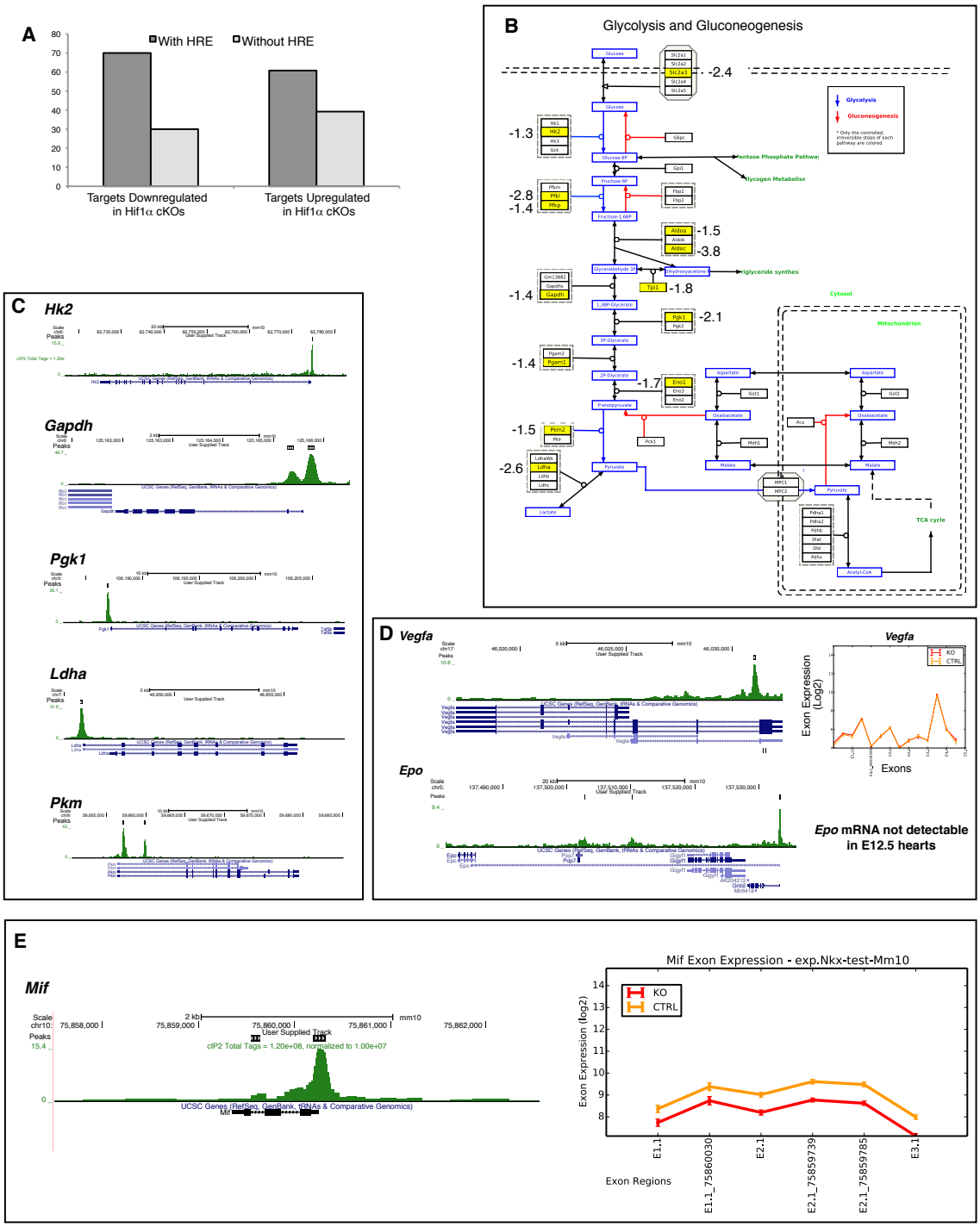


**Figure S3, Related to Figure 4. In fetal cardiomyocytes HIF1α directly activates expression of MIF, as well as enzymes and transporters involved in each step of glycolysis, but is not required for expression of angiogenic factors.**

**A)** Combined analysis of RNA-seq and ChIP-seq datasets revealed that 30% of downregulated and 39.2% of upregulated HIF1α target genes did not contain a minimal HIF binding sequence in the corresponding ChIP-seq peak, suggesting that HIF1α-mediated transcriptional regulation can take place independently of the presence of a classical hypoxia-responsive element (HRE). This observation is consistent with the results inferred from previous HIF1α ChIP-seq studies (Tanimoto et al., 2010). **B)** Schematic representation of the glycolytic cascade. Proteins encoded by genes that were directly bound by HIF1α and modulated in *Hif1a* cKO hearts are highlighted in yellow. Numbers represent fold-downregulation observed in mutants. **C)** Representative HIF1α ChIP-seq peaks in genes encoding glycolytic enzymes. **D)** ChIP-seq analyses revealed that, in fCMs, HIF1α bound to genomic loci surrounding genes encoding the angiogenic factors VEGF and EPO. These genes have been previously suggested to be activated by HIF1α (Grimm et al., 2002; Ryan et al., 2000). However, *Vegf* transcript levels were not significantly altered in *Hif1a* cKO hearts, as shown in the RNA-seq expression plot presented, and *Epo* mRNA was not detected at appreciable levels in E12.5 hearts. **E)** HIF1α-DNA binding was also observed 12 base-pairs upstream of the transcription start site of the *Mif* gene. Transcription of this gene encoding a well-characterized inhibitor of p53 activation (Fingerle-Rowson et al., 2003; Hudson et al., 1999) was significantly decreased in *Hif1a* cKO hearts, placing it as a target directly activated by HIF1α in fCMs, as previously suggested by others in mouse embryonic fibroblasts (Welford et al., 2006).

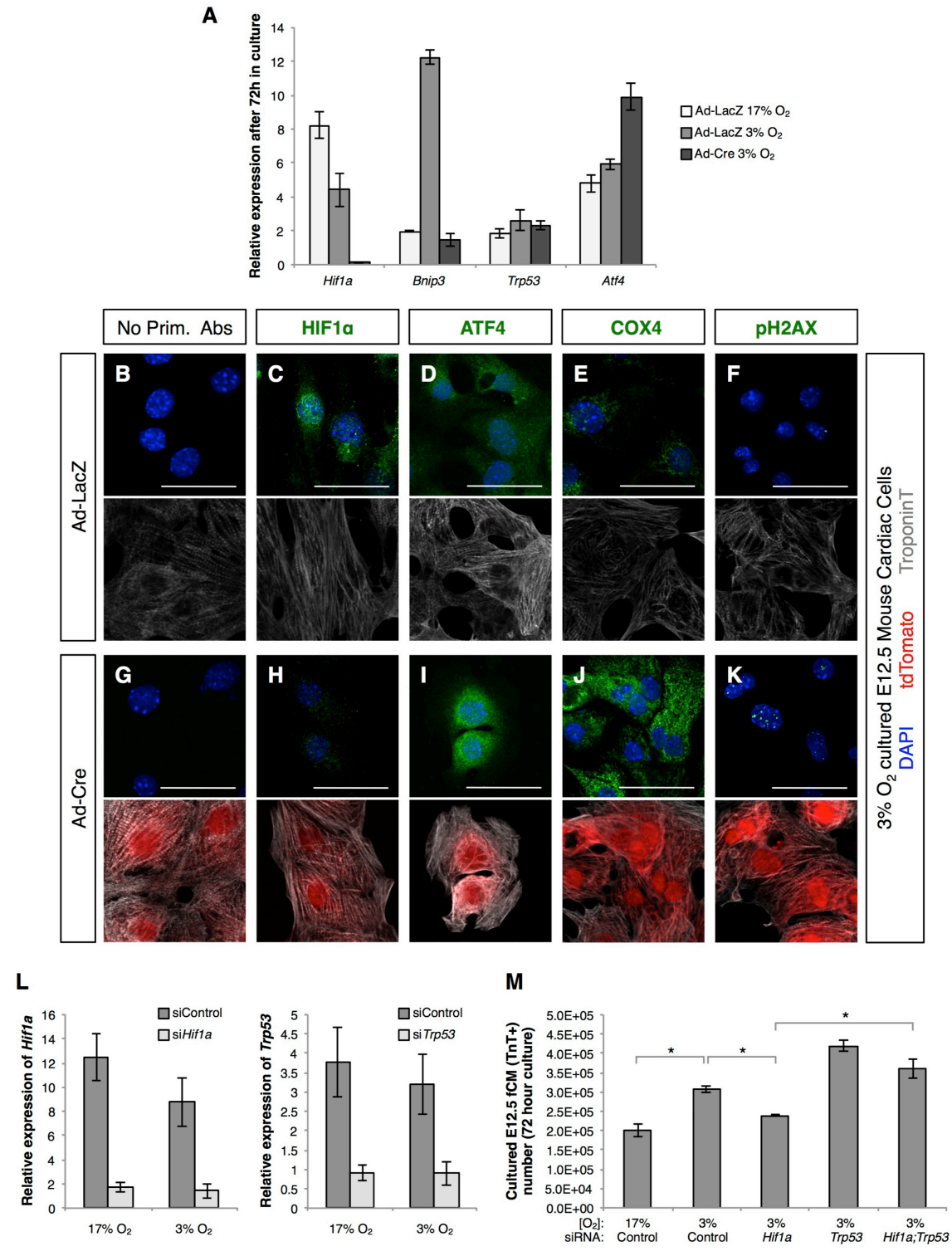


**Figure S4, related to Figure 5. A primary cell culture system that recapitulates *in vivo* consequences of ablation of HIF1α in fetal cardiomyocytes.**

E12.5 cardiac cells were isolated from the ventricles of *Hif1a*$^{fl/fl}$*; Rosa26*$^{tdTomato/tdTomato}$ embryos, infected with β-Galactosidase (Ad-LacZ) or Cre recombinase (Ad-Cre) expressing adenoviruses, cultured for 12 hours in normoxia to allow for degradation of HIF1α protein, and then cultured in 17% or 3% $O_2$ for an additional 48 hours. **A)** qPCR analyses showing that in cells cultured in 3% $O_2$, similar to what had been observed *in vivo,* excision of *Hif1a* lead to decreased expression of targets positively regulated by HIF1α (*Bnip3*) and increased expression of targets negatively regulated by HIF1α (*Atf4*), but produced no significant alterations in *Trp53* mRNA levels. **B-K)** Fluorescent immunocytochemistry of cells grown in 3% $O_2$ revealed that, when compared with LacZ transfected cells, *Hif1a*$^{fl/fl}$ fCMs transfected with Cre were depleted of HIF1α protein (**C** and **H**) and displayed molecular alterations that mimicked changes observed in *Nkx2-5*$^{Cre/WT}$; *Hif1a*$^{\Delta/fl}$ E12.5 embryos, namely: **D** and **I)** increased levels of ATF4; **E** and **J)** increased mitochondria biomass, as revealed by anti-COX4 staining; **F** and **K)** increased DNA damage, as revealed by anti-pH2AX staining. Note that, unlike Ad-LacZ treated cultures (B-F), Ad-Cre treated fCMs (G-K) displayed robust activation of the *Rosa26*$^{tdTomato}$ reporter, demonstrating the efficiency and specificity of this model for controlled recombination in primary fCM cultures. Bars represent 20 μm. **L and M)** To test the roles of HIF1α and p53 in the regulation of fCM proliferation, cultures of wild-type E12.5 ventricular cells were transfected with siRNAs targeting the mRNAs encoding these proteins and total numbers of fCMs were determined after 72h of culture in 17% or 3% $O_2$. **L)** qPCR validation of the efficiency of *Hif1a* and *Trp53* siRNAs in promoting the knockdown of their target mRNAs, regardless of the oxygen concentration cells were cultured in. **M)** Similar to the observations reported in Figure 5E-H, when cells were transfected with siControl, culture in 3% $O_2$ induced a significant increase in total fCM number relatively to culture in 17% $O_2$. This increase in fCM number was blunted by knocking down *Hif1a* and re-established when *Hif1a* and *Trp53* were knocked down simultaneously, suggesting that relative levels of these two transcription factors exert a rheostatic control over fCM proliferation. Target gene mRNA expression levels presented are relative to 18s RNA in the corresponding sample (ΔCt). A, L and M: data represented as mean +/- standard deviation; **P*<0.05.

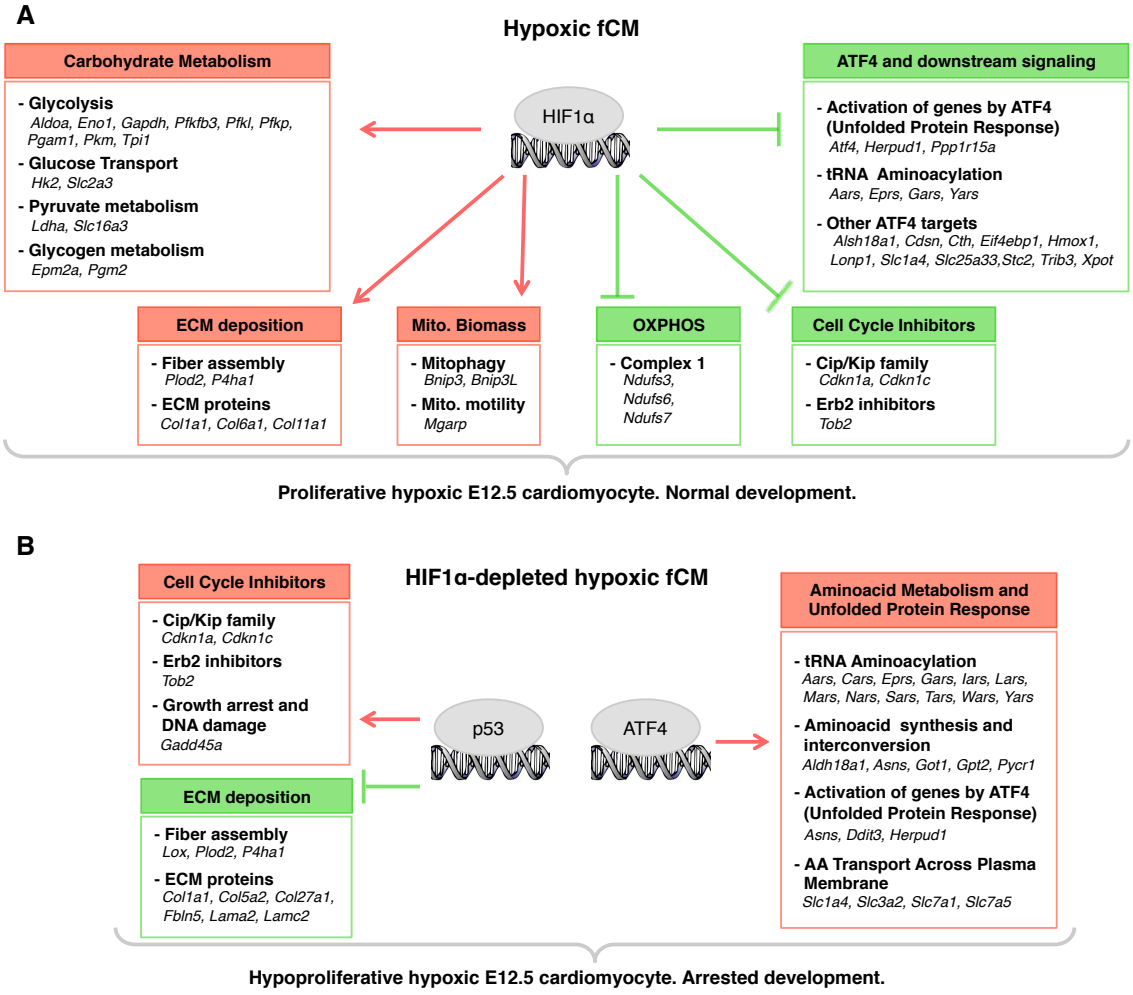


**Figure S5, related to Figure 6. Diagram listing all genes involved in the cellular processes highlighted in Figure 6.** Red color represents induction of gene expression and green represents transcriptional repression.

**Supplemental Tables**

**Table S1, related to Figure 1 – list of Affymetrix microarray datasets used for the elaboration of the heatmap presented in Figure 1.**

Microarray data listed was downloaded from the cardiogenomics website (http://cardiogenomics.med.harvard.edu) and processed according to the methodology described in the supplemental experimental procedures section. List of abbreviations: dn – dominant negative; h – hours; m – month; MI- myocardial infarction; NN – neo-natal; ntg – non-trangenic; w – weeks; y – year.

| Condition | # Arrays | Baseline | Array Type |
|---|---|---|---|
| Cardiac Development (E12.5,NN,1w,4w,5m,1y; n=3♂/group) | 18 | 1y♂, n=3 | U74Av1 |
| Gender (3m, 1y; n=3♀/group) | 6 | 1y♂, n=3 | U74Av1 |
| Dominant negative p21 Ras (n=3♀) | 3 | 3m, 1y♀, n=6 | U74Av1 |
| Aortic Banding (1h, 4h, 24h, 48h, 1w, 8w; n=3♂/group) | 36 | sham n=3♂/group | U74Av1 |
| PI3 kinase dn (n=3♀), ca (n=4♀) | 10 | PI3k ntg , n=3♀ | U74Av1 |
| Swimming | | | |
| 10min, 2.5d, 1w, 2w (n=3♀/group) | 15 | 8w, n=3♀ | U74Av2 |
| 3w, 4w (n=3♀/group) | 9 | 12w, n=3♀ | U74Av2 |
| 4w + 1w rest (n=3♀/group) | 6 | 13w, n=3♀ | U74Av2 |
| MI (1h, 4h, 24h, 48h, 1w, 8w) (n=3♀/group) | 36 | sham n=3♀/group | U74Av2 |
| MI Sham operation (1h, 4h, 24h, 48h, 1w, 8w) (n=3♀/group) | | 12w, 13w, n=6♀ | U74Av2 |
| IGF1R, IGF1R x PI3k dn, IGF1R x PI3k ca (n=3♀/group) | 9 | 12w, 13w, n=6♀ | U74Av2 |

**Table S2, related to Figure 4 – Characterization of the transcriptome of *Hif1a* cKO hearts and assessment of direct gene regulation by HIF1α. Data provided in a multi-tab Excel file.**

**A)** List of all genes significantly downregulated in *Hif1a* cKO hearts. **B)** List of all genes significantly upregulated in *Hif1a* cKO hearts. **C)** List of 2027 genes containing one or more HIF1α ChIP-seq peaks (peak score ≥ 3.5) and actively expressed in E12.5 hearts. **D)** List of all direct HIF1α targets significantly downregulated in *Hif1a* cKO hearts. **E)** List of all direct HIF1α targets significantly upregulated in *Hif1a* cKO hearts. **F)** Reactome analysis (Top 6 categories) for the genes listed in **A**, **B**, **D** and **E**. **G)** List of all HIF1α direct targets involved in regulating mitochondrial function modulated in *Hif1a* cKO hearts.

**Table S3, related to Figure 4 – Unfiltered list of all 17289 HIF1α ChIP-seq peaks annotated in E12.5 hearts. Data provided in an Excel file.**

**Table S4, related to Figure 4 – Bioinformatic prediction of putative HIF1α transcriptional partners.**

To search for candidate co-factors that might cooperate with HIF1α in the activation or repression of gene expression, the vicinities (+/- 100 bp) of HIF1α ChIP-seq peaks corresponding to targets modulated in *Hif1a* cKO hearts were screened for enrichment in transcription factor binding sequences. This analysis was independently performed for peaks with and peaks without hypoxia-responsive element (HRE). Sp1, a known HIF1α co-factor (Miki et al., 2004) is highlighted in purple. SMADs, previously proposed to function as an adaptor between HIF1 and SP1 (Sanchez-Elsner et al., 2002) are highlighted in gray, ATF4 in green, cardiac specific transcription factors in red and members of the ETS family in blue.

## Transcription factor binding sites enriched in HIF1α ChIP-seq peaks with HRE

| Name | P-value | q-value (Benjamini) | % Targets Sequences with Motif | % Background Sequences with Motif |
|---|---|---|---|---|
| **Downregulated in *Hif1a cKOs*** | | | | |
| HIF2a(bHLH)/785_O-HIF2a-ChIP-Seq(GSE34871) | 1.00E-73 | 0.0000 | 83.52% | 6.52% |
| HIF-1a(bHLH)/MCF7-HIF1a-ChIP-Seq(GSE28352) | 1.00E-57 | 0.0000 | 69.23% | 5.24% |
| HIF-1b(HLH)/T47D-HIF1b-ChIP-Seq(GSE59937) | 1.00E-54 | 0.0000 | 95.60% | 19.98% |
| Maz(Zf)/HepG2-Maz-ChIP-Seq(GSE31477) | 1.00E-04 | 0.0062 | 57.14% | 37.11% |
| TEAD4(TEA)/Tropoblast-Tead4-ChIP-Seq(GSE37350) | 1.00E-03 | 0.0516 | 13.19% | 4.57% |
| Sp1(Zf)/Promoter | 1.00E-03 | 0.0516 | 28.57% | 15.37% |
| TEAD(TEA)/Fibroblast-PU.1-ChIP-Seq | 1.00E-02 | 0.0516 | 8.79% | 2.24% |
| Smad3(MAD)/NPC-Smad3-ChIP-Seq(GSE36673) | 1.00E-02 | 0.1880 | 37.36% | 24.93% |
| CTCF-SatelliteElement/CD4+-CTCF-ChIP-Seq | 1.00E-02 | 0.1880 | 2.20% | 0.13% |
| Bach2(bZIP)/OCILy7-Bach2-ChIP-Seq(GSE44420) | 1.00E-02 | 0.2263 | 4.40% | 0.89% |
| **Upregulated in *Hif1a* cKOs** | | | | |
| HIF-1b(HLH)/T47D-HIF1b-ChIP-Seq(GSE59937) | 1.00E-07 | 0.0000 | 77.27% | 20.73% |
| HIF2a(bHLH)/785_O-HIF2a-ChIP-Seq(GSE34871) | 1.00E-07 | 0.0000 | 50.00% | 6.77% |
| HIF-1a(bHLH)/MCF7-HIF1a-ChIP-Seq(GSE28352) | 1.00E-06 | 0.0001 | 40.91% | 5.09% |
| Atf4(bZIP)/MEF-Atf4-ChIP-Seq(GSE35681) | 1.00E-04 | 0.0012 | 18.18% | 0.70% |
| Smad2(MAD)/ES-SMAD2-ChIP-Seq(GSE29422) | 1.00E-02 | 0.1154 | 45.45% | 17.28% |
| Smad4(MAD)/ESC-SMAD4-ChIP-Seq(GSE29422) | 1.00E-02 | 0.1594 | 45.45% | 18.55% |
| Egr2/Thymocytes-Egr2-ChIP-Seq(GSE34254) | 1.00E-02 | 0.2110 | 22.73% | 5.39% |
| ZNF143\|STAF(Zf)/CUTLL-ZNF143-ChIP-Seq(GSE29600) | 1.00E-02 | 0.2110 | 18.18% | 3.46% |

## Transcription factor binding sites enriched in HIF1α ChIP-seq peaks without HRE

| Name | P-value | q-value (Benjamini) | % Targets Sequences with Motif | % Background Sequences with Motif |
|---|---|---|---|---|
| **Downregulated in *Hif1a* cKOs** | | | | |
| ERG(ETS)/VCaP-ERG-ChIP-Seq | 1.00E-03 | 0.0946 | 35.90% | 13.69% |
| GABPA(ETS)/Jurkat-GABPa-ChIP-Seq | 1.00E-03 | 0.0946 | 25.64% | 7.74% |
| Mef2c(MADS)/GM12878-Mef2c-ChIP-Seq(GSE32465) | 1.00E-03 | 0.0946 | 20.51% | 5.06% |
| HEB?/mES-Nanog-ChIP-Seq | 1.00E-03 | 0.0946 | 17.95% | 4.12% |
| Mef2a(MADS)/HL1-Mef2a.biotin-ChIP-Seq/ | 1.00E-02 | 0.0946 | 17.95% | 4.44% |
| Gata4(Zf)/Heart-Gata4-ChIP-Seq(GSE35151) | 1.00E-02 | 0.0946 | 25.64% | 9.19% |
| Maz(Zf)/HepG2-Maz-ChIP-Seq(GSE31477) | 1.00E-02 | 0.1066 | 38.46% | 18.78% |
| Fli1(ETS)/CD8-FLI-ChIP-Seq(GSE20898) | 1.00E-02 | 0.1066 | 25.64% | 9.83% |
| Elk1(ETS)/Hela-Elk1-ChIP-Seq(GSE31477) | 1.00E-02 | 0.1116 | 17.95% | 5.38% |
| Elk4(ETS)/Hela-Elk4-ChIP-Seq(GSE31477) | 1.00E-02 | 0.1116 | 17.95% | 5.43% |
| ETV1(ETS)/GIST48-ETV1-ChIP-Seq | 1.00E-02 | 0.1170 | 28.21% | 12.19% |
| ETS1(ETS)/Jurkat-ETS1-ChIP-Seq | 1.00E-02 | 0.1333 | 23.08% | 9.04% |
| **Upregulated in *Hif1a* cKOs** | | | | |
| Ets1-distal(ETS)/CD4+-PolII-ChIP-Seq | 1.00E-03 | 0.0244 | 22.73% | 2.23% |
| EWS:ERG-fusion(ETS)/CADO_ES1-EWS:ERG-ChIP-Seq | 1.00E-02 | 0.4141 | 22.73% | 4.88% |
| GABPA(ETS)/Jurkat-GABPa-ChIP-Seq | 1.00E-02 | 0.6788 | 31.82% | 11.37% |

**Table S5, related to Figure 5 – Enrichment in ATF4 and p53 target genes amongst genes modulated in *Hif1a* cKO hearts. Data provided in a multi-tab Excel file.**

**A)** List of all ATF4 targets significantly upregulated in *Hif1a* cKO hearts. **B)** List of all p53 targets significantly upregulated in *Hif1a* cKO hearts. **C)** List of all p53 targets significantly downregulated in *Hif1a* cKO hearts. **D)** Reactome analysis (Top 5 categories) for the gene lists displayed in A-C. **E)** List of ATF4 and HIF1α common targets significantly upregulated in *Hif1a* cKO hearts. **F)** List of p53 and HIF1α common targets modulated in *Hif1a* cKO hearts.

## Supplemental Experimental Procedures

### Transgenic Animals

All animal care was in compliance with the *Guide for the Care and Use of Laboratory Animals* published by the US National Institutes of Health, as well as institutional guidelines at the University of California, San Diego. Mice were kept in IVC disposable cages (Innovive), under a 12-hour light cycle and maintained on a Black-Swiss (Taconic laboratories), C57BL/6J (Jackson Laboratory, stock number 000664) mixed background. The floxed *Hif1a* allele (Ryan et al., 2000) was purchased from the Jackson Laboratory (stock number 007561) and the null $Hif1a^{\Delta}$ allele was produced by crossing this line with the epiblastic *Meox2-Cre* strain (Jackson Laboratory, stock number 003755) (Tallquist and Soriano, 2000). *Nkx2-5-Cre* (Moses et al., 2001), *αMhc-Cre* (Abel et al., 1999), *Mlc2v-Cre* (Chen et al., 1998), *Wt1-Cre* (Wessels et al., 2012) and *Tie2-Cre* (Kisanuki et al., 2001) lines were kind gifts of Robert Schwartz, Dale Abel, Ju Chen, John Burch and Masashi Yanagisawa, respectively. For genotyping DNA was extracted from tail tip biopsies and amplified by PCR using the following primers: Cre_F – AATTTACTGACCGTACACCAAAA; Cre_R – CTATTTTCCATGAGTGAACGAAC for detection of Cre recombinase and Hif1a-F – GGAGCTATCTCTCTAGACC; Hif1a-R – GCAGTTAAGAGCACTAGTTG for detection of the floxed *Hif1a* allele. The null *Hif1a* allele was genotyped using Hif1a-R and a Hif1aNull-F primer– AAGCACCCAGTGCAAAGTAA. Developmental stage of embryos analyzed was classified as embryonic day (E) where noon of the vaginal plug day was considered as E0.5 and birth typically occurred at E19.

### Microarray dataset analysis

Affymetrix .cel files from 148 microarrays (Supplemental Table 1) were downloaded from the cardiogenomics website and normalized with RMA in R. Arrays were run on ventricular tissue from mice subjected to a variety of cardiac remodeling experimental paradigms, e.g. aortic banding timecourse, myocardial infarction timecourse, development timecourse, dilated cardiomyopathy, swimming induced hypertrophy timecourse (Table S1 - www.cardiogenomics.com). Expression ratios were generated from $Log_2$ signal values using each experimental control subtracted from the experimental condition and these were assessed for differentially expressed candidates with an F-test statistic using the multitest package in R (Dudoit et al., 2002). We

identified 7735 probesets as being differentially expressed (Westfall-Young adjusted permutation P<0.05). Differentially expressed transcripts were clustered using the HOPACH algorithm (van der Laan and Pollard, 2003) and first level clusters were annotated for Gene Ontology enrichment with the GO-Elite program (Zambon et al., 2012). To identify transcription factors that potentially regulate observed gene expression changes during cardiac development, we searched the 5kb promoters of gene clusters for enrichment of evolutionarily conserved (human to mouse) transcription factor binding sites in the TRANSFAC database as previously described (Zambon et al., 2005).

**Fluorescent immunohistochemistry/immunocytochemistry**

Embryos were isolated from timed pregnant females, fixed in 4% paraformaldehyde (Electron Microscope Sciences) overnight, dehydrated in a sucrose gradient and embedded in OCT (Sakura). Frozen embryos were sectioned (10μm thick) using a Leica CM3050S cryostat. Tissue sections or adherent cultured cells were incubated overnight with combinations of the following primary antibodies at the specified dilutions: rabbit polyclonal anti-HIF1α (NB100-479 lots V1 and W1, 1:200), mouse monoclonal anti-TroponinT (Thermo Scientific, clone 13-11, 1:100), goat polyclonal anti-FLK1 (R&D systems, AF644, 1:50), rabbit polyclonal anti-COX IV (Abcam, ab16056, 1:200), rabbit monoclonal anti-pH2AX (Ser139, Cell Signaling, clone 20E3, 1:100), rabbit polyclonal anti-ATF4 (Michael Kilberg, (Su and Kilberg, 2008), 1:100), rabbit anti-cleaved caspase 3 (Asp175, Cell Signaling, clone 5A1E, 1:200), rabbit polyclonal anti-MIF (Abcam, ab7207, 1:300), rabbit polyclonal anti-phospho Histone H3 (Ser10, Millipore, 06-570, 1:200). Primary antibodies were detected using AlexaFluor-conjugated (488, 555 or 647) donkey antibodies (Invitrogen), nuclei were counterstained with DAPI (Invitrogen) and slides mounted with fluorescent mounting medium (DAKO).

E12.5 mutant embryos were tested for efficiency of cardiac HIF1α ablation prior to downstream histological analyses. Embryos exhibiting inefficient protein depletion were excluded from our studies. For identification of proliferative cells, pregnant females received an IP injection of EdU (Invitrogen) 2 hours prior to embryo dissection and fluorescent detection of incorporated EdU was performed prior to primary antibody incubation, following manufacturer's instructions. For quantification of fetal cardiomyocyte proliferative indexes (Figure 3E), sections were stained for DAPI, FLK1, TroponinT and EdU. Five high magnification (160x) images were acquired for each area

analyzed (septum and compact myocardium). Nuclei of endothelial cells (nuclei surrounded by FLK1+ cytosol) were excluded from all quantifications. Total number of cardiomyocytes (nuclei surrounded by TroponinT+ cytosol) and number of proliferative cardiomyocytes (EdU+ nuclei surrounded by TroponinT+ cytosol) were quantified in medial sections from three mutants and three littermate controls. Results were plotted as ratio of proliferative cardiomyocytes/total cardiomyocyte number. Detection of apoptotic cells by TUNEL was carried using the In Situ Apoptosis Detection Kit (Takara) following manufacturer's instructions. Imaging was performed on an Olympus FV1000 confocal microscope and acquired images were edited using the Olympus software Fluoview.

**Assessment of timing of coronary perfusion**

To evaluate the timing at which the developing coronary vascular plexus connects to aortic blood flow, deciduas were isolated from timed pregnant females and transferred to a solution of HBSS supplemented with Heparin (10 units/mL, App Pharmaceutical). After embryo dissection, an incision was applied to the thoracic body wall and 10 µL of a 1:5 suspension of orange fluorescent (540/560) 0.1µm microspheres (Life Technologies, F8800) in HBSS/Heparin were injected into the left ventricle of each embryo using an insulin syringe (31G, BD Biosciences). Beating hearts were transferred to ice-cold 1x PBS for 10 minutes and further processed for histology as aforementioned.

**Sequencing of control and mutant transcriptomes (RNA-seq)**

Hearts from E12.5 embryos were rapidly dissected in ice cold 1x PBS and placed directly into TRIzol (Invitrogen), dounce homogenized (20 strokes) and total RNA isolated according to the manufacturer's instructions. Sequencing was conducted on an Illumina HiSeq2000 with paired end sequencing at 100 bp read length. Adapter and poor quality read sequences were trimmed with Trim Galore using default settings. Trimmed reads were quality controlled with FastQC (http://www.bioinformatics.bbsrc.ac.uk/projects/fastqc). On average each read pair resulted in ~55 million uniquely mapped reads after mapping to the Mm10 reference genome with TopHat2 (Kim et al., 2013) and Bowtie2 (Langmead and Salzberg, 2012). Transcript expression values were determined after transcript normalization (reads per kilobase per million reads–RPKM) with AltAnalyze (Salomonis et al., 2010). Functional clustering of modulated genes was performed using the REACTOME database (Croft et al., 2014).

**Quantitative RT-PCR**

Total RNA was isolated from cultured cells with TRIzol (Invitrogen) and converted to cDNA with a Super Script III cDNA Synthesis Kit (Invitrogen) according to the manufacturer's instructions. cDNA amplicons were quantified by incorporation of SYBR Green probe (KapaBioSystems, Inc.) into dsDNA. Primer sequences are indicated in the table bellow. Samples were compared using the relative (comparative) Ct method after adjusting for 18s RNA (ΔCt), using the following equation: Relative expression = $(2^{-\Delta Ct})x(1x10^5)$.

| | Forward | Reverse |
|---|---|---|
| *Hif1a* | ACCTTCATCGGAAACTCCAAAG | CTGTTAGGCTGGGAAAAGTTAGG |
| *Bnip3* | TCCTGGGTAGAACTGCACTTC | GCTGGGCATCCAACAGTATTT |
| *Trp53* | CTCTCCCCCGCAAAAGAAAAA | CGGAACATCTCGAAGCGTTTA |
| *Atf4* | CCTGAACAGCGAAGTGTTGG | TGGAGAACCCATGAGGTTTCAA |
| *18S* | GGTAACCCGTTGAACCCCATTCG | ACCATCCAATCGGTAGTAGCGACG |

**HIF1α ChIP-seq in E12.5 hearts**

E12.5 mouse hearts were dissected and cross-linked in 1.5% of formaldehyde methanol-free for 10 minutes at room temperature. Samples were quenched by incubation with 2.5M glycine for 5 minutes. Hearts were ressuspended in lysis buffer (50 mM HEPES-KOH pH 7.5; 140 mM NaCl; 1 mM EDTA; 10% Glycerol; 0.5% NP40; 0.25% Triton X-100) and dounce homogenized for nuclei isolation. The cross-linked chromatin was sonicated in Shearing buffer (1mM EDTA; 10mM Tris-HCl pH 7.6; 0.1% SDS) using a Covaris S2 (2% Duty cycle, 3 Intensity; 200 cycles per burst; for 8 minutes) to an average size of 200 bp. Precleared chromatin extract was incubated overnight at 4°C with 4µg of rabbit anti-HIF-1α antibody (Novus, NB100-479 lot V1) and immunoprecipitated with protein A–Sepharose beads. 10 ng of ChIP DNA were used to generate a standard Illumina sequencing library. Two biological replicates were generated and sequenced alongside one input library. Reads were mapped to Mm10 genome build with Bowtie2 and peaks were called using the Homer software (homer.salk.edu) with default settings with the exception that the P-value over input was reduced from <0.0001 to <0.05 (Heinz et al., 2010). Analysis of enrichment in

transcription factor binding sites in the vicinities of HIF1α ChIP-seq peaks was conducted using the Homer software.

**Isolation, culture and growth assessment of E12.5 ventricular cells**

E12.5 mouse ventricles were isolated from timed pregnant female Swiss Webster mice (Charles Rivers Laboratories) and placed directly in ice-cold 1X PBS. Ventricles from five litters were collected and then transferred to 7 mL ice-cold trypsin/EDTA for 15min. Hearts were enzymatically digested by 15 min of incubation at 37ºC with gentle inversion mixing every 5 min. At 15 minutes, single-cell suspensions were generated by gentle trituration. Cells were counted with a Scepter hand held cell counter using 40 µm tips and a setting of >8µm cell size (Millipore) and seeded at the indicated cell density in DMEM (DMEM, high glucose (Invitrogen), with additives: 1mM Sodium Pyruvate, 2mM L-glutamine, 20units/ml each penicillin/streptomycin, and 10% FBS). To determine cell growth, cells were rinsed twice with 1X PBS and enzymatic detached from tissue culture plastic with Detachin (Genlantis). Cells were counted with a Scepter hand held cell counter using 60 µm tips and a setting of >8µm cell size. Percentages of fCMs in each culture were determined by FACS using an anti-TroponinT antibody (Thermo Scientific, clone 13-11, 1:100). These numbers were multiplied by total cell counts to estimate total fCM numbers. For determination of ratios of proliferating fCMs, in addition to TroponinT, cell suspensions were stained for phospho-Histone H3 and analyzed by FACS. Evaluation of p53-DNA binding activity was performed using the TransAM p53 kit (Active Motif, 41196) and nuclear extracts freshly prepared from embryonic hearts or cultured ventricular cells.

For siRNA-mediated gene knockdown, $2.5x10^5$ cells/mL were plated in 35mm tissue culture dishes or 12 well plates. siRNA transfection was carried out using 2culsiRNA and 1.5µL Dharmafect I Transfection Reagent (Dharmacon) per well, according to manufacturer's protocol. Cells were transfected overnight in 17% $O_2$ and media changed the next morning. Upon media change, half the tissue culture dishes were transferred to 3% $O_2$ culture conditions. Cells were cultured for 72 hours and processed for cell counting as described above. siRNAs against *Hif1a* (D-040638-01-0005) and *Trp53* (D-040642-01-0005) were purchased from Dharmacon. Control siRNAs were purchased from Bioneer (SN-1013).

For the *ex vivo* knockout of HIF1α or HIF1α and p53, cells were isolated from $Hif1a^{fl/fl}$ or $Hif1a^{fl/fl};Trp53^{fl/fl}$ E12.5 ventricles, respectively, plated in 4-well chamberslides at a

density of 160 000 cells/well and transduced with Ad-LacZ or Ad-Cre adenoviruses overnight. To promote proteasomal degradation of HIF1α protein, incubation with viral particles was performed in 17% $O_2$. Twelve hours after, media was changed and half the chamberslides were transferred to 3% $O_2$ culture conditions. For assessment of DNA synthesis, 2.5μM EdU (Life Technologies) was added to the culture after incubation with viral particles. At the end of the experiment, cells were rinsed in 1x HBSS (Invitrogen), fixed in 4% paraformaldehyde (Electron Microscope Sciences) in HBSS for 15 minutes at room temperature and processed for fluorescent immunocytochemistry as aforementioned. For quantification of EdU incorporation (Figure 5H), cells were stained for EdU and TroponinT and seven 60x images were randomly acquired for each replicate (4 replicates per condition). Total number of cardiomyocytes (nuclei surrounded by TroponinT+ cytosol) and number of proliferative cardiomyocytes (EdU+ nuclei surrounded by TroponinT+ cytosol) were quantified using ImageJ (imagej.nih.gov). Results were plotted as ratio of proliferative cardiomyocytes/total cardiomyocyte number.

**Supplemental References**


Abel, E.D., Kaulbach, H.C., Tian, R., Hopkins, J.C.A., Duffy, J., Doetschman, T., Minnemann, T., Boers, M.-E., Hadro, E., Oberste-Berghaus, C*., et al.* (1999). Cardiac hypertrophy with preserved contractile function after selective deletion of GLUT4 from the heart. The Journal of Clinical Investigation *104*, 1703-1714.

Bellot, G., Garcia-Medina, R., Gounon, P., Chiche, J., Roux, D., Pouyssegur, J., and Mazure, N.M. (2009). Hypoxia-induced autophagy is mediated through hypoxia-inducible factor induction of BNIP3 and BNIP3L via their BH3 domains. Molecular and Cellular Biology *29*, 2570-2581.

Chen, J., Kubalak, S.W., and Chien, K.R. (1998). Ventricular muscle-restricted targeting of the RXRalpha gene reveals a non-cell-autonomous requirement in cardiac chamber morphogenesis. Development *125*, 1943-1949.

Compernolle, V., Brusselmans, K., Franco, D., Moorman, A., Dewerchin, M., Collen, D., and Carmeliet, P. (2003). Cardia bifida, defective heart development and abnormal neural crest migration in embryos lacking hypoxia-inducible factor-1α. Cardiovascular Research *60*, 569-579.

Croft, D., Mundo, A.F., Haw, R., Milacic, M., Weiser, J., Wu, G., Caudy, M., Garapati, P., Gillespie, M., Kamdar, M.R*., et al.* (2014). The Reactome pathway knowledgebase. Nucleic Acids Research *42*, D472-477.

Dudoit, S., Yang, Y.H., Callow, M.J., and Speed, T.P. (2002). Statistical methods for identifying differentially expressed genes in replicated cDNA microarray experiments. Stat Sinica *12*, 111-139.

Firth, J.D., Ebert, B.L., and Ratcliffe, P.J. (1995). Hypoxic regulation of lactate dehydrogenase A. Interaction between hypoxia-inducible factor 1 and cAMP response elements. The Journal of Biological Chemistry *270*, 21021-21027.

Fukuda, R., Zhang, H., Kim, J.W., Shimoda, L., Dang, C.V., and Semenza, G.L. (2007). HIF-1 regulates cytochrome oxidase subunits to optimize efficiency of respiration in hypoxic cells. Cell *129*, 111-122.

Grimm, C., Wenzel, A., Groszer, M., Mayser, H., Seeliger, M., Samardzija, M., Bauer, C., Gassmann, M., and Reme, C.E. (2002). HIF-1-induced erythropoietin in the hypoxic retina protects against light-induced retinal degeneration. Nature Medicine *8*, 718-724.

Haitina, T., Lindblom, J., Renstrom, T., and Fredriksson, R. (2006). Fourteen novel human members of mitochondrial solute carrier family 25 (SLC25) widely expressed in the central nervous system. Genomics *88*, 779-790.

Heinz, S., Benner, C., Spann, N., Bertolino, E., Lin, Y.C., Laslo, P., Cheng, J.X., Murre, C., Singh, H., and Glass, C.K. (2010). Simple combinations of lineage-determining transcription factors prime cis-regulatory elements required for macrophage and B cell identities. Molecular Cell *38*, 576-589.

Hudson, J.D., Shoaibi, M.A., Maestro, R., Carnero, A., Hannon, G.J., and Beach, D.H. (1999). A proinflammatory cytokine inhibits p53 tumor suppressor activity. The Journal of Experimental Medicine *190*, 1375-1382.

Iyer, N.V., Kotch, L.E., Agani, F., Leung, S.W., Laughner, E., Wenger, R.H., Gassmann, M., Gearhart, J.D., Lawler, A.M., Yu, A.Y.*, et al.* (1998). Cellular and developmental control of O2 homeostasis by hypoxia-inducible factor 1α. Genes & Development *12*, 149-162.

Kim, D., Pertea, G., Trapnell, C., Pimentel, H., Kelley, R., and Salzberg, S.L. (2013). TopHat2: accurate alignment of transcriptomes in the presence of insertions, deletions and gene fusions. Genome Biology *14*, R36.

Kim, J.W., Tchernyshyov, I., Semenza, G.L., and Dang, C.V. (2006). HIF-1-mediated expression of pyruvate dehydrogenase kinase: a metabolic switch required for cellular adaptation to hypoxia. Cell Metabolism *3*, 177-185.

Kisanuki, Y.Y., Hammer, R.E., Miyazaki, J., Williams, S.C., Richardson, J.A., and Yanagisawa, M. (2001). Tie2-Cre transgenic mice: a new model for endothelial cell-lineage analysis in vivo. Developmental Biology *230*, 230-242.

Langmead, B., and Salzberg, S.L. (2012). Fast gapped-read alignment with Bowtie 2. Nature Methods *9*, 357-359.

Li, Y., Lim, S., Hoffman, D., Aspenstrom, P., Federoff, H.J., and Rempe, D.A. (2009). HUMMR, a hypoxia- and HIF-1alpha-inducible protein, alters mitochondrial distribution and transport. The Journal of Cell Biology *185*, 1065-1081.

Madisen, L., Zwingman, T.A., Sunkin, S.M., Oh, S.W., Zariwala, H.A., Gu, H., Ng, L.L., Palmiter, R.D., Hawrylycz, M.J., Jones, A.R.*, et al.* (2010). A robust and high-throughput Cre reporting and characterization system for the whole mouse brain. Nature Neuroscience *13*, 133-140.

McKeller, M.R., Herrera-Rodriguez, S., Ma, W., Ortiz-Quintero, B., Rangel, R., Cande, C., Sims-Mourtada, J.C., Melnikova, V., Kashi, C., Phan, L.M.*, et al.* (2010). Vital function of PRELI and essential requirement of its LEA motif. Cell Death & Disease *1*, e21.

Miki, N., Ikuta, M., and Matsui, T. (2004). Hypoxia-induced activation of the retinoic acid receptor-related orphan receptor alpha4 gene by an interaction between hypoxia-inducible factor-1 and Sp1. The Journal of Biological Chemistry *279*, 15025-15031.

Moses, K.A., DeMayo, F., Braun, R.M., Reecy, J.L., and Schwartz, R.J. (2001). Embryonic expression of an Nkx2-5/Cre gene using ROSA26 reporter mice. Genesis *31*, 176-180.

Pagliarini, D.J., Calvo, S.E., Chang, B., Sheth, S.A., Vafai, S.B., Ong, S.E., Walford, G.A., Sugiana, C., Boneh, A., Chen, W.K.*, et al.* (2008). A mitochondrial protein compendium elucidates complex I disease biology. Cell *134*, 112-123.

Papandreou, I., Cairns, R.A., Fontana, L., Lim, A.L., and Denko, N.C. (2006). HIF-1 mediates adaptation to hypoxia by actively downregulating mitochondrial oxygen consumption. Cell Metabolism *3*, 187-197.

Ryan, H.E., Lo, J., and Johnson, R.S. (1998). HIF-1α is required for solid tumor formation and embryonic vascularization. The EMBO Journal *17*, 3005-3015.

Salomonis, N., Schlieve, C.R., Pereira, L., Wahlquist, C., Colas, A., Zambon, A.C., Vranizan, K., Spindler, M.J., Pico, A.R., Cline, M.S.*, et al.* (2010). Alternative splicing regulates mouse embryonic stem cell pluripotency and differentiation. Proceedings of the National Academy of Sciences of the United States of America *107*, 10514-10519.

Sanchez-Elsner, T., Botella, L.M., Velasco, B., Langa, C., and Bernabeu, C. (2002). Endoglin expression is regulated by transcriptional cooperation between the hypoxia and transforming growth factor-beta pathways. The Journal of Biological Chemistry *277*, 43799-43808.

Su, N., and Kilberg, M.S. (2008). C/EBP homology protein (CHOP) interacts with activating transcription factor 4 (ATF4) and negatively regulates the stress-dependent induction of the asparagine synthetase gene. The Journal of Biological Chemistry *283*, 35106-35117.

Tallquist, M.D., and Soriano, P. (2000). Epiblast-restricted Cre expression in MORE mice: a tool to distinguish embryonic vs. extra-embryonic gene function. Genesis *26*, 113-115..

Tello, D., Balsa, E., Acosta-Iborra, B., Fuertes-Yebra, E., Elorza, A., Ordonez, A., Corral-Escariz, M., Soro, I., Lopez-Bernardo, E., Perales-Clemente, E.*, et al.* (2011). Induction of the mitochondrial NDUFA4L2 protein by HIF-1alpha decreases oxygen consumption by inhibiting Complex I activity. Cell Metabolism *14*, 768-779.

van der Laan, M.J., and Pollard, K.S. (2003). A new algorithm for hybrid hierarchical clustering with visualization and the bootstrap. J Stat Plan Infer *117*, 275-303.

Wessels, A., van den Hoff, M.J., Adamo, R.F., Phelps, A.L., Lockhart, M.M., Sauls, K., Briggs, L.E., Norris, R.A., van Wijk, B., Perez-Pomares, J.M.*, et al.* (2012). Epicardially derived fibroblasts preferentially contribute to the parietal leaflets of the atrioventricular valves in the murine heart. Developmental Biology *366*, 111-124.

Zambon, A.C., Gaj, S., Ho, I., Hanspers, K., Vranizan, K., Evelo, C.T., Conklin, B.R., Pico, A.R., and Salomonis, N. (2012). GO-Elite: a flexible solution for pathway and ontology over-representation. Bioinformatics *28*, 2209-2210.

Zambon, A.C., Zhang, L., Minovitsky, S., Kanter, J.R., Prabhakar, S., Salomonis, N., Vranizan, K., Dubchak, I., Conklin, B.R., and Insel, P.A. (2005). Gene expression patterns define key transcriptional events in cell-cycle regulation by cAMP and protein kinase A. Proceedings of the National Academy of Sciences of the United States of America *102*, 8561-8566.

Zhang, H., Bosch-Marce, M., Shimoda, L.A., Tan, Y.S., Baek, J.H., Wesley, J.B., Gonzalez, F.J., and Semenza, G.L. (2008). Mitochondrial autophagy is an HIF-1-

dependent adaptive metabolic response to hypoxia. The Journal of Biological Chemistry *283*, 10892-10903.